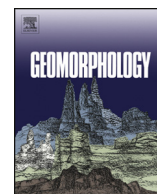




Contents lists available at ScienceDirect

Geomorphology

journal homepage: www.elsevier.com/locate/geomorph

Detailed mapping of shallow landslides in eastern Oklahoma and western Arkansas and potential triggering by Oklahoma earthquakes

Netra R. Regmi ^{*}, Jacob I. Walter

Oklahoma Geological Survey, The University of Oklahoma, Norman, OK, United States of America

ARTICLE INFO

Article history:

Received 30 September 2018

Received in revised form 6 May 2019

Accepted 6 May 2019

Available online xxxx

Keywords:

Eastern Oklahoma

Shallow landslides

LiDAR data

Surface roughness

ABSTRACT

Landslides have long been considered one of the main erosive drivers that sculpt hillslopes over time. Tectonic forces raise slopes that can be sculpted by climate and the degree to which they can be sculpted depends upon the underlying lithology and hillslope geomorphology. Landslides destroy life and property and contribute to the evolution of mountain landscapes by generating and transporting hillslope sediments. In this study, we investigate the dynamics of soil-mantled hillslopes in eastern Oklahoma and western Arkansas, USA, by mapping shallow landslides, evaluating the frequency and magnitude of the landslides, and quantifying the surface geometries.

We mapped 185 shallow landslides in a 150 km² area. The approximate ages of landslides and the frequencies and magnitudes (area, volume and runout) were estimated using historical aerial photographs. The landslide database was then used to compute rate of landslide occurrence and sediment yield. In addition, landslide surface geometries, including slope, curvature and surface roughness, were determined from 10 m NED and 2 m LiDAR elevation data. The hillslope susceptibility studies, derived from elevation data, were augmented by our review of common historical accounts that link landslides in the study region to the 1952 M 5.4 El Reno, Oklahoma earthquake ~300 km away. In light of that case study, we determined the frequency of historical earthquakes that impart >2 kPa dynamic stresses for the study area since 1900 and find an increased potential for dynamic stress perturbation of landslide activity since ~2010. All these characteristics were then evaluated to understand the dynamics of hillslopes and hillslope susceptibility to shallow landslides.

Frequency assessment of mapped landslides suggested that frequency of landslides increased significantly during 2005–2016 compared to 1995–2005. On average ~10 shallow landslides occurred every year during 2005–2016. These landslides alone contributed $\sim 1.5 \times 10^5$ m³/yr (sediment yield rate: ~ 0.10 mm/yr) of sediments. Surface roughness values were relatively higher in landslide areas compared to that of surrounding non-landslide areas. The surface roughness index mapped ~84% of observed landslides, and suggests that the index could be used to map hillslope susceptibility to landslides for future planned studies.

Published by Elsevier B.V.

1. Introduction

The interaction of climate and tectonic forces with underlying lithology determines hillslope sediment mobilization and slope morphology, which controls sediment transport shaping hillslopes and depositing sediment in stream channels and lowlands (Ahnert, 1970; Dietrich et al., 2003). Studies carried out in various climate and geological environments have recognized that climate, tectonics, and underlying lithology and structure can drive differences in the rate of sediment production and transport, and ultimately the evolution of hillslope morphology (Kessler et al., 2006; Istanbuluoglu et al., 2008; Tucker and Hancock, 2010; Poulos et al., 2012; Pelletier et al., 2013; McGuire et al., 2014; Regmi et al., 2014a). The mechanism of interaction,

however, among climate, seismicity and underlying lithology and landslides and erosion as process-response is not well-understood in the subtropical ecosystem of eastern Oklahoma and western Arkansas, USA, where the mountains are mostly soil-mantled and dominated by deformed sandstone and shale. Here, we address this knowledge gap using a combination of empirical field observations and aerial photographic mapping of shallow landslides, and hillslope geomorphic analyses using high resolution digital elevation models (DEMs). The study characterizes various attributes of historical landslides including age, area, runout, and volume; determines temporal frequency of historical earthquakes that imparted >2 kPa dynamic stresses for the study area, and finally uses these attributes to characterize susceptibility of hillslopes to shallow landslides.

The objective of this study was to understand the dynamics of hillslopes in subtropical climatic mountainous areas in eastern Oklahoma and western Arkansas. Specifically, we: (1) mapped shallow

^{*} Corresponding author.

E-mail address: netraregmi@ou.edu (N.R. Regmi).

landslides and quantified the frequency, magnitude, and rate of sediment production; (2) determined various slope geometries, including slope, curvature, and surface roughness, and determined the relationships with landslides; and (3) evaluated the hillslope susceptibility to shallow landslides. Because landslides are a hazard to life and property in our study area, our observations may shed light onto the susceptibility to landslides, which are a significant public hazard.

2. The study area

2.1. Climate

The study area is in the Ouachita Mountains in eastern Oklahoma and western Arkansas (Fig. 1). The area is characterized by a humid subtropical climate, driven by the warm, moist air moving northward from the Gulf of Mexico (Oklahoma Climatological Survey, 2018). Based on the analysis of climatic data from 1971 to 2000, the annual average temperature is $\sim 16^\circ\text{C}$, and the annual average precipitation is $\sim 120\text{--}130\text{ cm}$ (Johnson and Luza, 2008). The area receives maximum precipitation during summer (June, July and August) and minimum precipitation during winter (December, January and February) (see Johnson and Luza, 2008 for details).

2.2. Geology and geomorphology

Geology in the area is dominated by the Pennsylvanian lithology, including sandstone and shale of the Boggy, Savana, McAlester, and Hartshorne formations and Quaternary alluvial and terrace deposits (Hemish and Suneson, 1997; Heran et al., 2003). The study covers two mountains in Oklahoma with outcropping Boggy and Savana formations, and a mountain in Arkansas consisting of the Savana Formation. Both formations consist of thin-bedded, deformed fine- to medium-grained sandstones, and thick-bedded, weathered, and organic-rich fossiliferous shales. Both formations also contain limestone and coal. Lowlands around these mountains, underlain by McAlester and

Hartshorne formations and Quaternary terraces, alluvial and colluvial deposits, are not the focus of this study. The area exhibits a few faults and a regional NE-SW trending synclinal structure known as Cavanal syncline.

Slopes underlain by shale are predominantly soil-mantled and concave in nature, whereas slopes underlain by sandstone exhibit relatively convex geometry. Most of the soil-mantled slopes exhibit characteristic soil creeping (Fig. 2), whereas sandstone exposures exhibit rock falls and rockslides that deposit large amounts of colluvial material at the base of the slopes. Soil-mantled slopes consist of soils developed primarily by the weathering of shale, and colluvium deposited by erosion and landslides. Shale is highly weathered and the resulting soil is cohesive in nature, whereas colluvial deposits consist of rock fragments and boulders, and thereby are relatively frictionally stronger and able to maintain a higher angle of repose. The average depth of the soil is observed as $>1\text{ m}$ in most of the landscapes, particularly along the zones of topographic convergence (i.e., hillslope hollows or topographic depressions) (Figs. 2 and 3).

The vegetation in the area is primarily oak-pine forest in upland areas and post-oak blackjack forest in lowlands. Upland vegetation consists primarily of various Oak species and shortleaf pine, and associated vegetation includes trees and shrubs including flowering dogwood, highbush and lowbush blueberries, hophorn beam, redbud serviceberry, and sugar maple (Johnson and Luza, 2008).

2.3. Historical earthquakes and landslides

Oakes (1952) describes eyewitness reports of landslides along Cavanal Hill shortly after the April 9, 1952 El Reno earthquake, a M 5.5 earthquake that occurred $\sim 300\text{ km}$ from Cavanal Hill. Those observations, reported in a newsletter published by the Oklahoma Geological Survey, suggest a direct triggering link between the landslide and distant earthquake. Dynamic triggering by passing surface waves is the most plausible cause that would trigger a landslide at a distance of $\sim 300\text{ km}$. Surface waves from distant earthquakes have the ability to

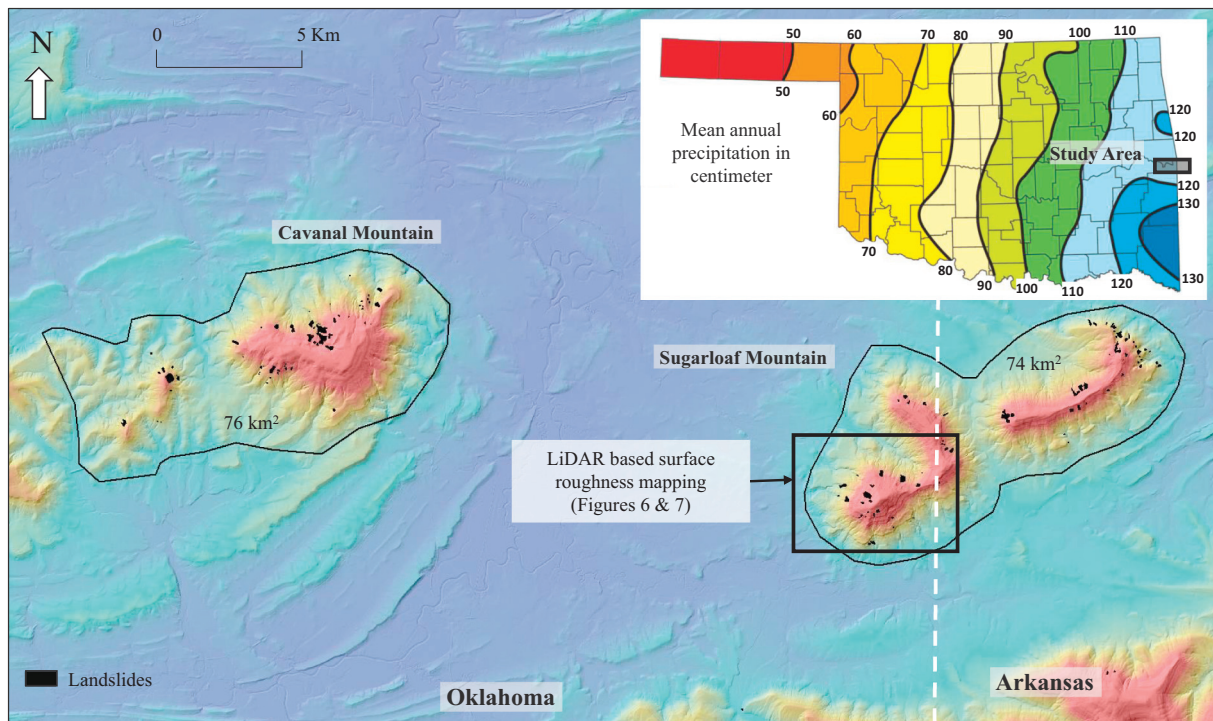


Fig. 1. Location of the study area (150 km^2), which comprises two mountains in eastern Oklahoma and a mountain in western Arkansas. The map in the upper right corner shows the mean annual precipitation (inches) in Oklahoma based on 1971–2000 precipitation data (modified after Johnson and Luza, 2008).

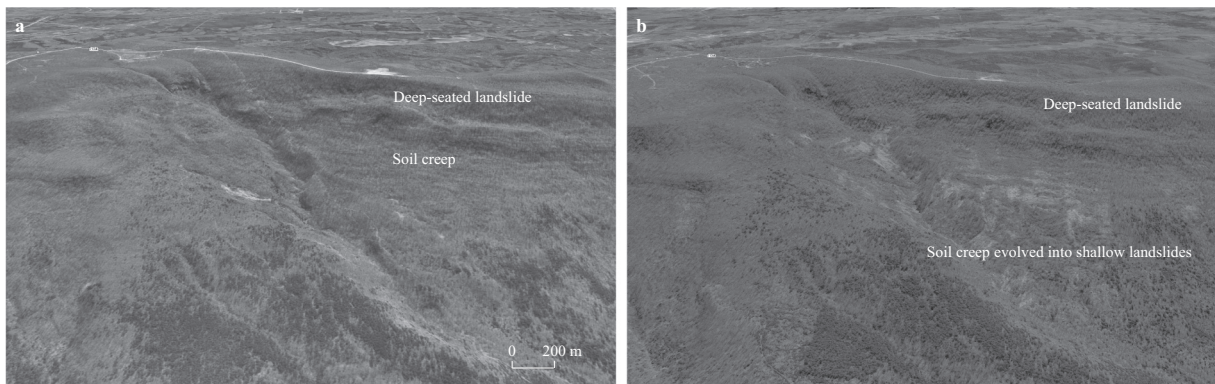


Fig. 2. Aerial photographs showing a part of study area in (a) 1995 and (b) 2016. The soil-mantled hillslope seems to be in steady state creeping in 1995. Observations from 2012 and 2016 aerial photographs suggested that the hillslope evolved into shallow landslides during the 2012–2016 period.

trigger local earthquakes, volcanic eruptions, geyser activity, glacier calving and landslides (Meier et al., 1984; Rodriguez et al., 1999; Hill and Prejean, 2007).

Landslides during earthquakes can be a substantial secondary hazard that can cause damage and casualties (Rodriguez et al., 1999). The dynamic stress changes from passing surface waves cause a momentary stress perturbation that may trigger slope failure on slopes that are precariously or critically-stressed. These factors may be enhanced during wet weather when soils are saturated and more prone to failure (Chang et al., 2007).

The rate of earthquakes across the mid-continent part of the United States has dramatically increased since 2009. The historically high rates of seismicity across the mid-continent have been largely driven by substantial increases in seismicity occurring within Oklahoma. In the intervening years, Oklahoma has experienced several moderate and damaging earthquakes including the November 2011 M_w 5.7 Prague earthquake (Keranan et al., 2013), the September 2016 M_w 5.8 Pawnee earthquake (Walter et al., 2017; Yeck et al., 2017), and the November 2016 M_w 5.0 Cushing earthquake. These earthquakes occurred in an area that prior to 2009 background tectonic rates were about two

M 3.0+ earthquakes per year, which increased to 579 and 903 M 3.0+ earthquakes in 2014 and 2015, respectively.

The increase in seismicity in Oklahoma was roughly coincident with the last oil and gas boom focused around the Mississippian Limestone and Hunton Limestones. Those formations contain substantial amounts of co-produced formation brines and widespread use of horizontal production wells and hydrofracturing led to vast amounts of brines to dispose. Common disposal practices involved disposing of wastewater in deep underground injection wells completed into upper parts of the basement and the karst Arbuckle Group, which directly overlies the basement. From 2010 to late 2014, statewide rates of disposal increased from ~4.8 million cubic meter/month to ~14.3 million cubic meter/month (OCC Data, last accessed August 2018). The increase in the rate of seismicity roughly corresponded to the increase in monthly rates of injection, though with sometimes a lag greater than a year or so in many sub-regions of Oklahoma (Langenbruch and Zoback, 2016; Goebel et al., 2017). That observation, coupled with the depth of the seismicity mostly occurring within basement rocks and sometimes along previously-mapped basement faults has led to the general

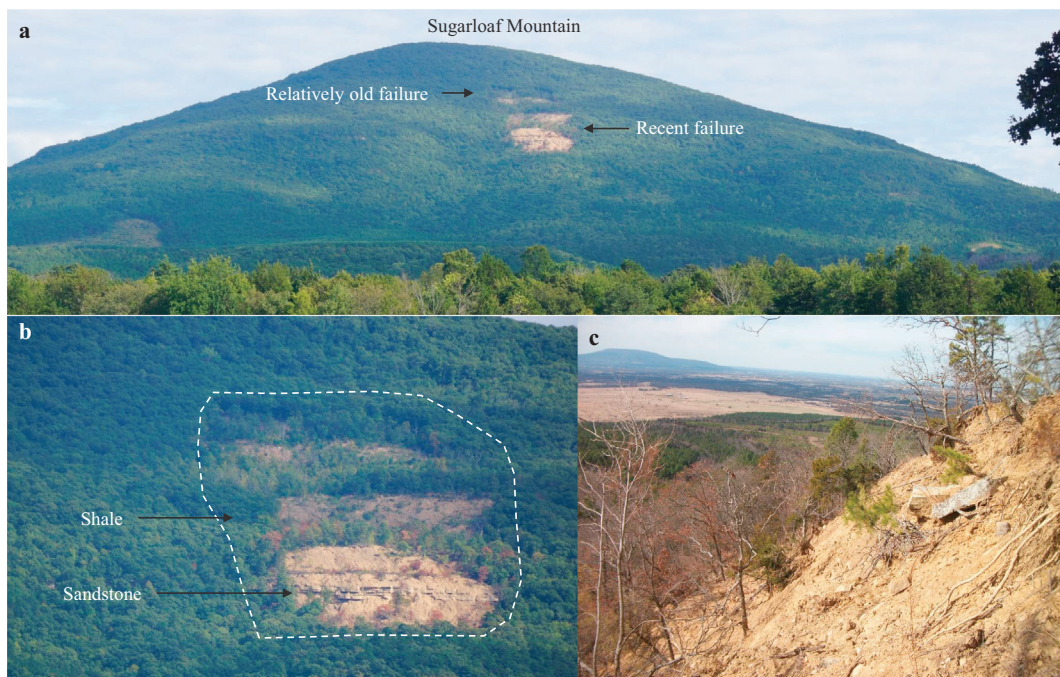


Fig. 3. Photographs showing a recent landslide in Sugarloaf Mountain. (a) A large landslide in Sugarloaf Mountain. (b) The closeup view of the landslide showing the thin sandstone layer and the thick shale-derived soil (>1 m). (c) The view of the landslide scarp. Photographs taken in early September 2018 by David Deaton and Steve Humphries.

consensus within the scientific community that wastewater disposal was inducing earthquakes across Oklahoma since at least 2010 (Walsh and Zoback, 2015).

2.4. Landslides and erosion

Very few studies on mass movement have been conducted in the study area (Oakes, 1952; Webb, 1960; He et al., 2014), in spite of the clear evidence of various mass movement and erosional features including old deep-seated landslides, recent shallow landslides, soil creeps, rills, gullies and incised first and higher order channels. Deep-seated landslides are large, and exhibit surface morphology similar to that of large slump-block style landslides (Baum and Odum, 1996). Large deep-seated landslides, found mostly on the edges of the upland plateau (Fig. 2), appear to be related to the structural failure of the bedrock. These landslides are densely vegetated and have smooth surfaces with well-evolved hydrological network, indicating that these landslides are probably hundreds- to thousands of years old and relatively stable now (LaHusen et al., 2016). The headscarps of some of the large deep-seated landslides contain active shallow landslides. Deep-seated landslides are beyond the scope of this study. These landslides could have occurred in completely different climatic and tectonic conditions, and could be the result of completely different mechanisms than that of shallow landslides that are the subject of this study.

Shallow landslides, defined here as landslides with depth of slip surface less than the tree root depth (<10 m), are classified following Varnes (1978). They include soil creep and soil slides mostly on soil-mantled surfaces underlain by shale; debris flows along zones of topographic convergence underlain mostly by shale; and debris slides mostly in colluvial deposits. Rockslides and rock falls also occur, particularly on steep slopes formed by sandstone exposure and contribute to the development of colluvial deposits at the base of the slope.

3. Materials and methods

3.1. Datasets used

We utilized aerial photographs acquired from 1995 to 2018, 1:250,000 scale USGS geological map of the area (Marcher, 1969), 10 m National Elevation Dataset (NED) (<https://nationalmap.gov/elevation.html>), and 2 m LiDAR topographic data acquired in 2010 (<https://nationalmap.gov/elevation.html>). The approximate ages of landslides were assessed from aerial photographs. Slope geometries were mapped from the NED and LiDAR elevation data. Field mapping was carried out to verify the map of landslides and for detailed characterization of slope geometries and underlying soil and lithology. Global and regional earthquake catalogs, reported since 1900, were collected to evaluate dynamic stress from passing surface waves imparted upon the study area. The dynamic stress values and the earthquake frequencies were then assessed qualitatively to explain the likelihood of the occurrence of earthquake triggered landslides.

3.2. Landslide mapping

Landslides were identified and mapped as polygons on aerial photographs based on tonal and textural characteristics, similar to other recent studies (Regmi et al., 2010a; Garcia-Urquia and Yamagishi, 2017). The approximate ages were determined from 1995 to 2016 aerial photographs available in Google Earth Pro, and the areas and runout lengths were computed in ArcGIS® (ESRI, Redland, CA). Landslide volumes were computed based on the volume (V) and area (A) relationship proposed for North Fork Gunnison River catchment of western Colorado (Regmi et al., 2014a):

$$V = 0.0254 \times A^{1.45} \quad (1)$$

We consider the equation is applicable for this study because the geologic and geomorphic environments in Cavanal and Sugarloaf Mountains are similar to that of North Fork of Gunnison River catchment. The type and geometries of some landslides were verified in the field.

3.3. Surface geomorphic analysis

Surface geometries including slope and curvature were calculated using 10 m NED topographic data in ArcGIS® using a 3 cell × 3 cell (30 × 30 m) moving window (see ESRI (2016) and Regmi et al. (2013) for equations). The local slope gradient (m/m) and curvature (1/m) of hillslopes were then regressed with drainage area calculated from DEM using the D8 algorithm (Fairfield and Leymarie, 1991) to differentiate valley head, hillslope and fluvial process domains and to characterize ridge-valley profiles (Montgomery and Dietrich, 1988; Kirby and Whipple, 2001; Istanbuluoglu et al., 2008; Regmi, 2010; McGuire et al., 2014). Landslide scarps were differentiated and average slope and curvature of landslide scarps in each process domain were computed and compared with slope and curvature process domains.

High resolution 2 m LiDAR topographic data across a portion of the study area (Fig. 1) was used to compute surface roughness. The surface roughness was computed as a standard deviation of slope using a 5 cell × 5 cell (10 × 10 m) moving window, following Regmi et al. (2014b). We then tested the usefulness of surface roughness in mapping landslides assuming (1) active surfaces of landslides, soil creeps, and erosion develop characteristic surface geometries, such as hummocks, and irregular surface topography formed by the displacement and accumulation of slope materials; and (2) surface roughness of these features tends to be higher compared to that of relatively stable surrounding areas. The efficacy of this test was determined based on the plot of the percentage of the study area from high to low surface roughness (x-axis) versus the percentage of landslides (y-axis), following Regmi et al. (2010a). The accuracy of the model was then determined by computing the area under the curve (AUC) of the plot. The AUC out of the total area covered by the curve explains the overall prediction accuracy of the model. Surface roughness characterizes soil-geomorphic processes and hazards of Quaternary alluvial fans (Frankel and Dolan, 2007; Regmi et al., 2014b; Regmi and Rasmussen, 2018), and mountain slopes (Glenn et al., 2006; LaHusen et al., 2016).

3.4. Earthquake dynamic stresses for the study area

To analyze the magnitude of dynamic stress change from passing surface waves from distant earthquakes, we combined earthquake catalogs for worldwide large earthquakes globally since 1900 from the Advanced National Seismic System (ANSS) and in Oklahoma from the Oklahoma Geological Survey (OGS). The reason behind the hybrid approach is that smaller magnitude earthquakes within close proximity can create dynamic stresses equivalent to larger, more distant earthquakes. If a seismometer had been installed near the study area, we could have estimated dynamic stress from the peak ground velocity of that hypothetical instrument. Because no such instrument existed in the study area, we followed the approach of Van Der Elst and Brodsky (2010) and estimated dynamic stresses in a piecewise sense for distant and closer earthquakes. For distant earthquakes (epicentral distance >800 km from the study region), we first estimated surface wave amplitudes at the study area using an equation proposed by Van Der Elst and Brodsky (2010):

$$\log_{10} A_{20} = M_S - 1.66 \log_{10} \Delta - 2 \quad (2)$$

where Δ is the epicentral distance in degrees, A_{20} is the peak surface-wave displacement at a period of 20 s and M_S is the surface wave magnitude. For simplification, we assumed that the earthquake

magnitude is equal to M_s and estimated peak ground velocity (\dot{u}) following [Chao et al. \(2013\)](#):

$$\dot{u} = 2\pi A_{20}/T \quad (3)$$

We assumed a nominal value of 35 GPa for the shear modulus (G) and 3.5 km/s phase velocity for Rayleigh waves (v), and estimated the dynamic stress ($\Delta\sigma$) from $\Delta\sigma = G\dot{u}/v$ ([Hill and Prejean, 2007](#)). For closer earthquakes (epicentral distance <800 km from the study region), we follow equations outlined in the aforementioned paper ([Van Der Elst and Brodsky, 2010](#)).

4. Results

4.1. Landslide characteristics and age

Area and runout of the observed shallow landslides range from 64 to 55,000 m² and 11 to 500 m, respectively ([Table 1](#)). Volumes computed based on Eq. (1) proposed by [Regmi et al. \(2014a\)](#) range from 11 to 260,000 m³. Average slope of the landslides is $19 \pm 7^\circ$, significantly higher than the average slope of the entire area ($11 \pm 7^\circ$) ([Table 2](#)). Curvature analysis suggests, however, that average values of landslide surface curvature and the entire area curvature are similar ([Table 2](#)).

The approximate ages of 137 landslides out of 185 were successfully determined from aerial photographs acquired in different times from 1995 to 2016 ([Table 1](#)) and archived in Google Earth. The ages of 48 landslides, however, were difficult to determine because the size of landslides were nearly equivalent to the resolution of older aerial photographs or landslide surfaces were covered by dense vegetation. In addition, only 25 identified landslides occurred prior to 2000 and only four landslides occurred during 2000–2005. We identified 46 landslides between 2005 and 2010, and 62 landslides between 2010 and 2016. We only consider the inventory of landslides after 2005 to assess the rate of landslide occurrence and sediment yield. The frequency distribution of landslides over 2005–2016 indicates that ~10 landslides occur every year with landslide density of ~0.7 landslides per square kilometer. The sediment volume produced by landslides during that period (2005–2016) was $\sim 1.5 \times 10^5$ m³/yr, and the sediment yield rate is ~0.10 mm/yr.

4.2. Landslide distribution and hillslope and channel characteristics

The slope-area plot identifies three process domains including valley heads, hillslopes and channels ([Fig. 4a](#)). The plot suggests that ~7% (13) of total landslide scarps are located in valley heads (drainage area <200 m²) and ~92% (170) of total landslide scarps are located in hillslopes (drainage area 200–80,000 m²). Slope gradients of landslide scarps averaged by the drainage area on a logarithmic scale are significantly higher than that of valley head and hillslope process domains. The curvature-area plot indicates that mostly first and second order channels are steep and concave, however, the convexity of the higher order channels increases downstream ([Fig. 4b](#)). The plot also indicates that the curvature of landslide scarps averaged by the drainage area is similar to that of process domains.

Table 1

Observation of shallow landslide characteristics across the study area.

Approx. age	No. of landslides	Area (m ²)			Modeled volume (m ³)				Sed. yield (m ³ /yr)	Sed. yield (mm/yr)
		Min	Mean	Max	Min	Mean	Max	Sum		
Prior to 2000	25	147	6761	68,388	35	16,979	260,350	424,466	NA	NA
2000–2005	4	2008	3084	5092	1562	3046	6024	12,184	2437	0.00
2005–2010	46	143	7880	55,101	34	15,916	190,335	732,122	146,424	0.10
2010–2016	62	245	7394	46,010	74	14,854	146,545	920,963	153,494	0.10
Unknown	48	64	2500	29,852	11	4267	78,260	204,798	NA	NA
Entire landslides	185	64	6066	68,388	11	12,403	260,350	2,294,533	NA	NA

Table 2

Hillslope characteristics of shallow landslides and the entire area.

	Slope (°)		Curvature (1/m)		Surface roughness (°)	
	Mean	SD	Mean	SD	Mean	SD
Shallow landslides	19	7	-0.25	3	4.1	2
Entire area	11	7	0.001	2	2.3	2

Acronyms: SD: Standard deviation.

4.3. Earthquake frequency and dynamic stress

The 1952 El Reno earthquake imposed an ~16 kPa dynamic stress near the study area and the 2011 Prague and 2016 Pawnee earthquakes imparted dynamic stresses of ~39 and ~34 kPa, respectively ([Fig. 5a](#)). These values are much higher than the apparent triggering threshold of ~1 kPa for a triggered tremor at Parkfield and small local earthquakes ([Peng et al., 2009, 2014](#)). Based on a review of triggering across a number of studies, [Hill and Prejean \(2007\)](#) suggest a threshold ~2 kPa for triggering local earthquakes or other tectonic phenomena. Because that value may trigger earthquake faulting, we used it rather arbitrarily for the threshold for possible shallow landslide triggering. Individual landslide occurrence is inherently time-aliased because of the time between visible imagery collection, thus, we simply evaluated the annual frequency of earthquakes imposing dynamic stress changes >2 kPa near the study area. Based on methods described in [Section 3.4](#), we calculated dynamic stresses from distant and local earthquakes and determined the number of earthquakes per year that exceed the 2 kPa dynamic stress threshold ([Fig. 5b](#)). With this rate, we computed the 5-yr moving average to smooth the dataset. Our results show that the frequency of earthquakes that can impart significant dynamic stresses on the study area increased in the 2010s ([Fig. 5b](#)), concurrent with the dramatic increase in earthquakes in Oklahoma in the last decade.

4.4. Surface roughness and landslide susceptibility

The surface roughness map derived from the LiDAR topographic data ([Figs. 6 and 7, Table 2](#)), shows high roughness values in (1) landslide surfaces including scarps and deposits, and undulated surface topography developed by soil creeps; (2) rills, gullies, incised first and higher order channels, ridges, and spurs; and (3) steep sandstone bedrock slopes. The majority of landslides were observed primarily in three landscape positions including: (1) soil-mantled concave slopes underlain by shale; (2) colluvial deposits at the base of steep sandstone bedrock slopes; and (3) in proximity with the incised first and second order channels. Some landslides, particularly rockslides and rock falls, were observed in steep sandstone bedrock slopes. Some landslides were observed as evolving from soil creep ([Fig. 2](#)); and some landslides were observed in sandstone and shale transitions, probably caused by the difference in the shear strengths. A map of surface roughness predicted all these areas with high values of surface roughness ([Figs. 6 and 7](#)). In addition, the roughness map also identified hummocky topography resulting primarily from old landslide deposits, active surfaces

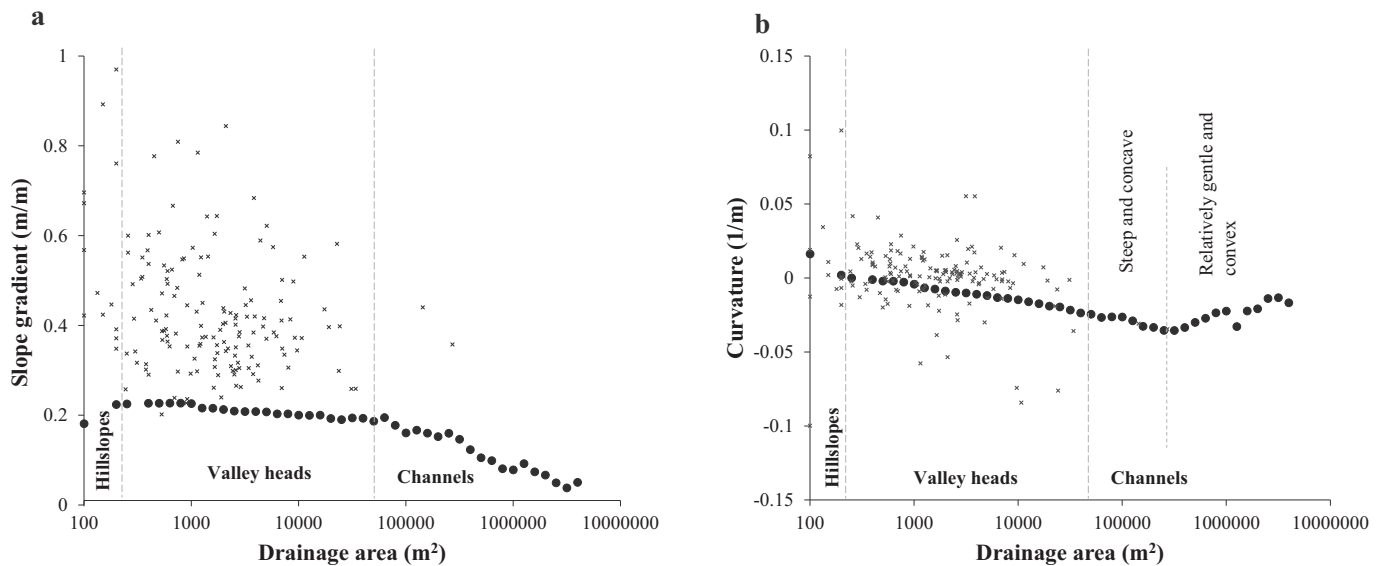


Fig. 4. Plots showing geomorphic characteristics of hillslopes, channels and landslides. (a) Local slope-drainage area plot. (b) Local curvature-drainage area plot. Average gradient and curvature of slopes were plotted as solid circles and landslide scarps were plotted as asterisks against drainage areas. Note, the plot shows 13 landslides (7%) occur in valley heads and 170 landslides (~90%) on hillslopes.

of soil creeps, and sediments accumulated by rock falls and rockslides (Figs. 6 and 7). The surface roughness map can be used as an indicator for first order characterization of unstable hillslope areas for mapping hillslope susceptibility to shallow landslides and erosion. Fig. 8, which is a plot of the percentage of the study area from high to low surface roughness versus percentage of landslides suggests that the surface roughness technique maps ~84% ($AUC = 0.84$) of the observed landslides.

5. Discussion

5.1. Landslide characteristics and sediment dynamics

This study represents a regional perspective on one of the more active landscapes in eastern Oklahoma and western Arkansas where climatic and seismic forces act together over deformed lithology and results in various types of mass movement, erosion, and stream incision (Oakes, 1952; Webb, 1960). The hilly landscape, consisting of

alternating layers of sandstone and shale, exhibits a geomorphic dichotomy where thin sandstone layers maintain the slope, and thick shale undergoes relatively intense weathering, rapid soil development, erosion, channel incision, soil creeping, and episodic landsliding, thereby creating a concave slope profile. On closer inspection, the area contains dominant, underlying geomorphic sculpting by a few large, deep-seated landslides that are probably hundreds to thousands of years old, which are plausibly related to structural failures of bedrock.

Frequency and sediment yield assessment of shallow landslides that occurred during 2005–2016 (Table 1) indicates that on average ~10 landslides with the spatial density of ~0.7/km² occur each year. These landslides alone produce ~0.10 mm/yr of sediment. This density and rate of sediment yield is within the range of published rates of landslide density and hillslope denudation in many tectonically active terrains of the world (Lavé and Burbank, 2004; Roering et al., 2007; Regmi et al., 2010b; Palumbo et al., 2011; Regmi et al., 2014a), suggesting that the slopes are active and landslides are one of the major processes that yield and transport huge amounts of sediment each year in the study

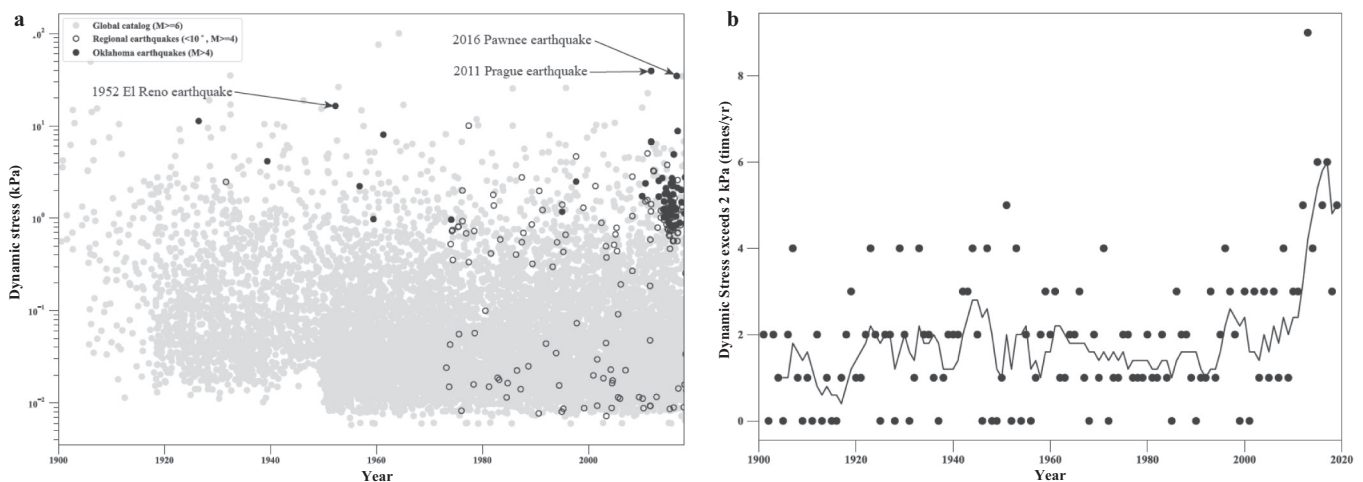


Fig. 5. Dynamic stress and frequency of major historical earthquakes. (a) Dynamic stress at the study area from distant earthquakes since 1900, including global earthquakes ($M \geq 6.0$; light gray), regional earthquakes (within 10° and $M \geq 4.0$), and Oklahoma earthquakes ($M \geq 4.0$ from the OGS catalog). (b) Frequency (per year) that earthquakes exceed a dynamic stress of 2 kPa within the study area. Solid black line indicates the frequency with a 5-yr running average.

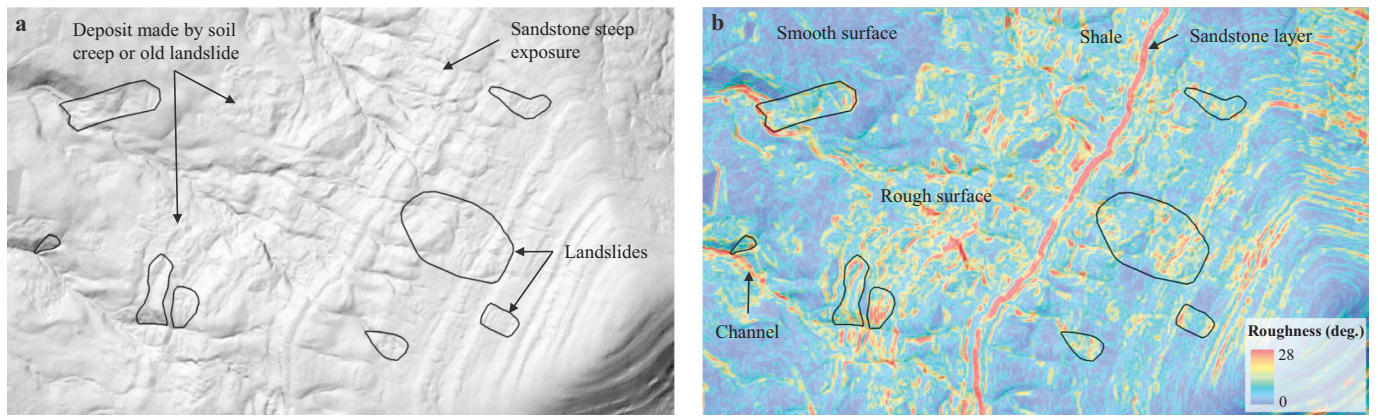


Fig. 6. Two-meter LiDAR DEM-derived hillslope geometries. (a) Hill-shaded image showing landslide polygons and various other landforms and (b) surface roughness map computed as a standard deviation of slope in 10 m × 10 m moving window.

area. For comparison, sediment yield is 0.15 mm/yr in very active hillslopes of Rocky Mountains in western Colorado using similar methods to those utilized in this manuscript (Regmi et al., 2014a). Similarly, results show the convexity of channels increases downstream (Fig. 4b), which is plausibly the result of sediment accumulation.

We consider precipitation, soil susceptibility, and dynamic triggering by distant earthquakes the major factors that cause shallow landslides in the study area. Southeast Oklahoma receives more precipitation than any other area of the state (Fig. 1). The majority of the slopes in the area are soil-mantled, underlain by soil derived from shale and sandstone. Deposits derived from sandstone are mostly frictional, whereas in situ soil developed by the weathering of shale has considerable cohesion because of the presence of clay and organics. Additionally, the area has dense vegetation that contributes to the development of thick soil profiles consisting of organic rich horizons that have relatively fine-grained texture and well-developed structure (Kay and Lal, 1998). In such environments, the subsurface also exhibits well-developed tree root associated flowpaths and drainage networks. The combined effect of these attributes results in higher infiltration, conductivity and moisture potential of soil (Easter et al., 1991), which

during storms facilitates building up of pore-water pressure, and, thereby, landslides and erosion.

We consider three potential explanations for the increase in the frequency of observed landslides for 2005–2016, compared to 1995–2005 (Table 1). It is possible that the aerial photographs and other data are not sufficient to map all landslides prior to 2005 because of the coarser resolution of aerial photographs and surfaces of landslides that could have smoothed out as a feedback-response of hydrological, weathering, vegetation, and soil-biotic processes (Guthrie and Evans, 2007; LaHusen et al., 2016). Second, very high precipitation was recorded in eastern Oklahoma during 2016 (Oklahoma Climatological Survey, 2018), and this could have triggered some of the observed landslides. Third, landslides could have been triggered by the Pawnee, Prague, Cushing, and other recent Oklahoma earthquakes occurring nearby since 2010 (Fig. 5).

5.2. Contribution of climatic and seismic forces in shallow landslides

Although landslides in the eastern Oklahoma have been reported as being associated with intense precipitation (Oakes, 1952; Webb, 1960;

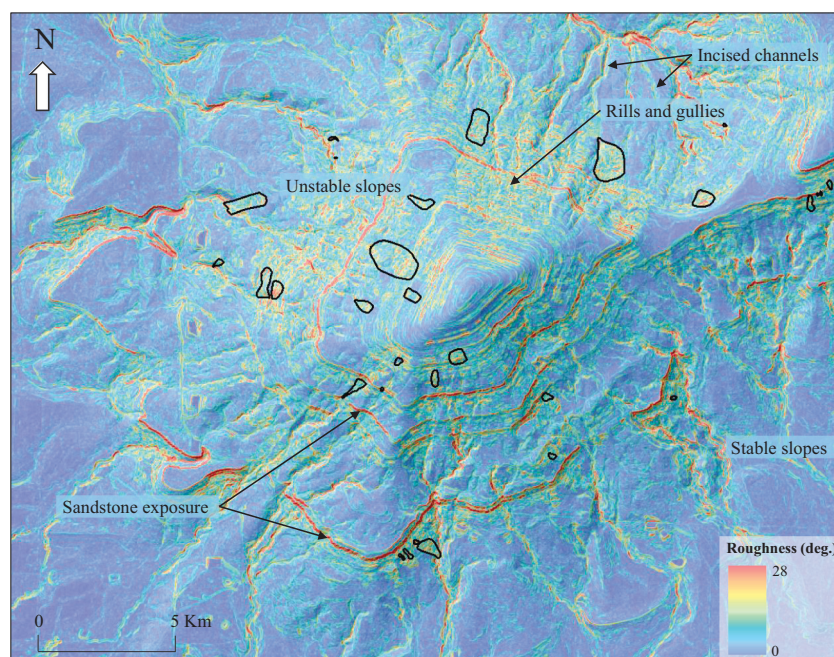


Fig. 7. Landslide polygons overlaid over surface roughness map of hillslope in a part of the study area (See Fig. 1).

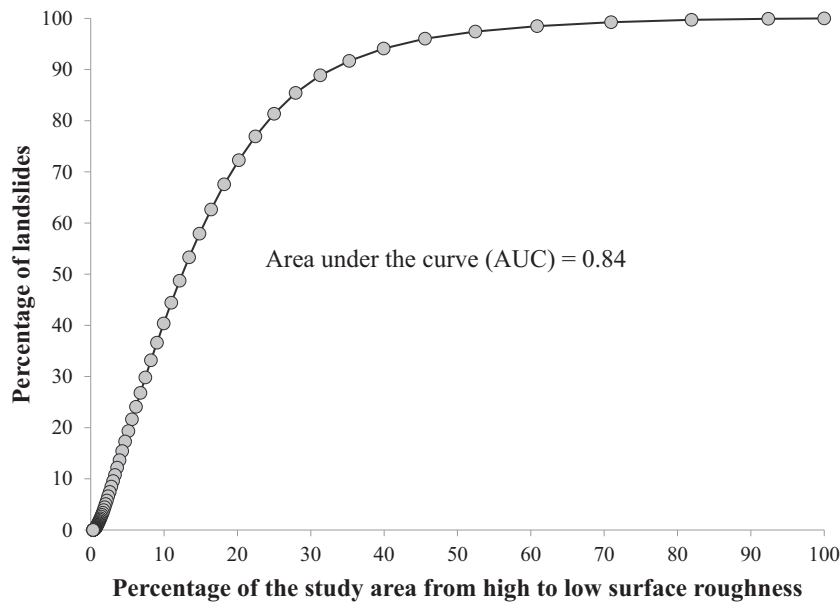


Fig. 8. A plot showing the shallow landslide prediction by surface roughness. Note that the percentage of landslides were plotted against the percentage of the study area from high to low surface roughness. The area under the curve (AUC) characterizes the overall prediction accuracy of the model.

He et al., 2014), dynamic triggering by distant earthquakes could have triggered the mass movements. Near the study area, at least one notable earthquake occurred, the M 5.4 El Reno Earthquake (April 9, 1952) that triggered landslides in Cavanal Mountain. The timing of the earthquake was such that it occurred during a time of year (April 9) with intense seasonal precipitation (Oakes, 1952). Fig. 5a suggests that the dynamic stresses imparted by the Prague Earthquake (2011) and the Pawnee Earthquake (2016) are more than two times greater than the El Reno Earthquake (Fig. 5a). Although we have no data up to this point to support that those earthquakes induced any landslides in the study area, it is very likely that these earthquakes could have triggered some landslides, and the frequency of landslides that increased significantly after 2010 could be associated with these events. In addition, the El Reno Earthquake occurred during the wet season (Fig. 5b), and it is very likely that the cumulative effect of the earthquake and the precipitation could have generated the 1952 landslide. This raises another concern that an earthquake similar to the magnitude of the Pawnee, Prague or Cushing earthquakes during the wet season likely would trigger landslides in the area.

Hillslopes in the study area are underlain by thick soil rich in organics and clay. The majority of these hillslopes also exhibit soil creep, which could be the result of soil deformation by frequent seismic shaking and seasonal fluctuations in pore-water pressure (Seed and Chan, 1966; Kirkby, 1967; Roering et al., 1999). Many shallow landslides were observed as evolved from soil-creep (Fig. 2), suggesting that hillslopes with soil creep can produce rapid landslides given appropriate environmental conditions, such as seismic shaking and/or intense precipitation (Roering et al., 1999). Seismic shaking may simply act to promote large-scale slope failures if other conditions are met.

5.3. Surface roughness as an indicator of landslide and erosion susceptibility

The surface roughness map indicates that the surface signatures of shallow landslides, soil creeps, and sediments deposited by old landslides, rock falls, and erosion are well captured by higher surface roughness values. The index also characterizes erosional features including rills and gullies, as well as steep landslide and erosion susceptible slopes in close proximity to channels as high surface roughness values. This illustrates that the index can be used as a mapping tool for the first order

identification of active and hazardous slopes. Similar kinds of indices have successfully been used in mapping landslides in different geologic, climatic and tectonic regions worldwide (McKean and Roering, 2004; Booth et al., 2009; Grohmann et al., 2011; Berti et al., 2013; LaHusen et al., 2016), and this study provides additional insights in the efficacy of the index in mapping shallow landslides. This study shows the index identified ~84% of the observed landslides, which is as good as the other studies that used a number of environmental covariates and robust statistical approaches in mapping landslide hazards and susceptibility worldwide (Lee et al., 2002; Van Westen et al., 2003; Lee and Choi, 2004; Mathew et al., 2007; Dahal et al., 2008).

6. Conclusions

Upland slopes in eastern Oklahoma and western Arkansas have long been recognized as susceptible to landslides and erosion because of the underlying deformed and weathered lithology and intense or seasonal precipitation (Oakes, 1952; Webb, 1960; He et al., 2014). We explored the possibility that more frequent shaking by distant earthquakes in the last decade may have also increased the frequency of landslides. We find a qualitative synchronicity between an increase in Oklahoma earthquakes in the last decade that would be sufficiently large to generate large dynamic stresses in the study area and an increase in the frequency of landslides over roughly the same period. This study suggests that upland slopes underlain by shale and sandstone in the area (i.e., Cavanal Hill) are highly dynamic and susceptible to landslides, soil creeps and erosion, similar to studies that suggested the susceptibility of weathered shale to landslides in different climatic and geological environments (Ohlmacher and Davis, 2003; Chigira et al., 2010). These slopes yield large amounts of sediment by landslide processes and highlight the importance of considering the characteristics of shale and sandstone stratigraphy in decision making in mitigation of landslides and management of hillslopes in eastern Oklahoma.

LiDAR elevation-derived surface roughness successfully mapped existing landslides and additional unstable landforms, such as hummocky topography developed by landslides, soil creep and colluvium, and steep slopes in close proximity to the first and higher order channels, which suggests that the tool is applicable in automatically mapping unstable hillslopes.

Acknowledgment

We are grateful to David Brown, Neil Suneson and Julie Chang of Oklahoma Geological Survey for their valuable suggestions. We thank David Deaton and Steve Humphries for providing photographs of recent landslides in Sugarloaf Mountain.

References

- Ahnert, F., 1970. Functional relationships between denudation, relief, and uplift in large mid-latitude drainage basins. *Am. J. Sci.* 268 (3), 243–8.
- Baum, R.L., Odum, J.K., 1996. Geologic Map of Slump-Block Deposits in Part of the Grand Mesa Area, Delta and Mesa Counties, Colorado 2331-1258.
- Berti, M., Corsini, A., Daehne, A., 2013. Comparative analysis of surface roughness algorithms for the identification of active landslides. *Geomorphology* 182, 1–18.
- Booth, A.M., Roering, J.J., Perron, J.T., 2009. Automated landslide mapping using spectral analysis and high-resolution topographic data: Puget Sound lowlands, Washington, and Portland Hills, Oregon. *Geomorphology* 109 (3–4), 132–147.
- Chang, K.-T., Chiang, S.-H., Hsu, M.-L., 2007. Modeling typhoon-and earthquake-induced landslides in a mountainous watershed using logistic regression. *Geomorphology* 89 (3–4), 335–347.
- Chao, K., Peng, Z., Gonzalez-Huizar, H., Aiken, C., Enescu, B., Kao, H., Velasco, A.A., Obara, K., Matsuzawa, T., 2013. A global search for triggered tremor following the 2011 M_w 9.0 Tohoku earthquake. *Bull. Seismol. Soc. Am.* 103 (2B), 1551–1571.
- Chigira, M., Wu, X., Inokuchi, T., Wang, G., 2010. Landslides induced by the 2008 Wenchuan earthquake, Sichuan, China. *Geomorphology* 118 (3–4), 225–238.
- Dahal, R.K., Hasegawa, S., Nonomura, A., Yamanaka, M., Dhakal, S., Paudyal, P., 2008. Predictive modelling of rainfall-induced landslide hazard in the Lesser Himalaya of Nepal based on weights-of-evidence. *Geomorphology* 102 (3–4), 496–510.
- Dietrich, W.E., Bellugi, D.G., Sklar, L.S., Stock, J.D., 2003. Geomorphic transport laws for predicting landscape form and dynamics. In: Wilcock, P.R., Iverson, R.M. (Eds.), *Prediction in Geomorphology*. Geophys. Monogr. Ser. AGU, Washington, D.C., pp. 103–132.
- Easter, K.W., Dixon, J.A., Hufschmidt, M.M., 1991. *Watershed Resources Management: Studies from Asia and the Pacific*. Institute of Southeast Asian Studies.
- ESRI, 2016. ArcGIS Desktop: Release 10. Environmental Systems Research Institute, Redlands, CA.
- Fairfield, J., Leymarie, P., 1991. Drainage networks from grid digital elevation models. *Water Resour. Res.* 27 (5), 709–717.
- Frankel, K.L., Dolan, J.F., 2007. Characterizing arid region alluvial fan surface roughness with airborne laser swath mapping digital topographic data. *Journal of Geophysical Research: Earth Surface* 112 (F2).
- García-Urquía, E., Yamagishi, H., 2017. Landslide Susceptibility Mapping Based on Aerial Photograph Interpretation Inventory for Tegucigalpa, Honduras: An Application of the Matrix Method, GIS Landslide. Springer, pp. 163–181.
- Glenn, N.F., Streutker, D.R., Chadwick, D.J., Thackray, G.D., Dorsch, S.J., 2006. Analysis of LiDAR-derived topographic information for characterizing and differentiating landslide morphology and activity. *Geomorphology* 73 (1–2), 131–148.
- Goebel, T.H., Walter, J.I., Murray, K., Brodsky, E.E., 2017. Comment on “How will induced seismicity in Oklahoma respond to decreased saltwater injection rates?” by C. Langenbruch and MD Zoback. *Sci. Adv.* 3 (8), e1700441.
- Grohmann, C.H., Smith, M.J., Ricomini, C., 2011. Multiscale analysis of topographic surface roughness in the Midland Valley, Scotland. *IEEE Trans. Geosci. Remote Sens.* 49 (4), 1200–1213.
- Guthrie, R., Evans, S., 2007. Work, persistence, and formative events: the geomorphic impact of landslides. *Geomorphology* 88 (3), 266–275.
- He, X., Hong, Y., Yu, X., Cerato, A.B., Zhang, X., Komac, M., 2014. Landslide susceptibility mapping in Oklahoma state using GIS-based weighted linear combination method. *Landslide Science for a Safer Geoenvironment*. Springer, pp. 371–377.
- Hemish, L.A., Suneson, N.H., 1997. Stratigraphy and Resources of the Krebs Group (Desmoinesian) South-Central Arkoma Basin. 30. Oklahoma Geological Survey Guidebook, p. 84.
- Heran, W.D., Green, G.N., Stoesser, D.B., 2003. A digital geologic map database for the state of Oklahoma. U.S. Geological Survey Open-File Report 03–247.
- Hill, D.P., Prejean, S., 2007. Dynamic triggering. In: Kanamori, H. (Ed.), *Treatise on Geophysics: Earthquake Seismology 4*. Elsevier, Amsterdam, pp. 257–291.
- Istanbulluoglu, E., Yetemen, O., Vivoni, E.R., Gutierrez-Jurado, H.A., Bras, R.L., 2008. Eco-geomorphic implications of hillslope aspect: inferences from analysis of landscape morphology in central New Mexico. *Geophys. Res. Lett.* 35 (14).
- Johnson, K.S., Luza, K.V., 2008. Earth Sciences and Mineral Resources of Oklahoma. Oklahoma Geological Survey.
- Kay, B., Lal, R., 1998. Soil structure and organic carbon: a review. *Soil Processes and the Carbon Cycle*. 198, pp. 169–197.
- Keranen, K.M., Savage, H.M., Abers, G.A., Cochran, E.S., 2013. Potentially induced earthquakes in Oklahoma, USA: links between wastewater injection and the 2011 M_w 5.7 earthquake sequence. *Geology* 41 (6), 699–702.
- Kessler, M.A., Anderson, R.S., Stock, G.M., 2006. Modeling topographic and climatic control of east-west asymmetry in Sierra Nevada glacier length during the last Glacial Maximum. *J. Geophys. Res.-Earth* 111 (F2).
- Kirby, E., Whipple, K., 2001. Quantifying differential rock-uplift rates via stream profile analysis. *Geology* 29 (5), 415–418.
- Kirkby, M., 1967. Measurement and theory of soil creep. *The Journal of Geology* 75 (4), 359–378.
- LaHusen, S.R., Duvall, A.R., Booth, A.M., Montgomery, D.R., 2016. Surface roughness dating of long-runout landslides near Oso, Washington (USA), reveals persistent postglacial hillslope instability. *Geology* 44 (2), 111–114.
- Langenbruch, C., Zoback, M.D., 2016. How will induced seismicity in Oklahoma respond to decreased saltwater injection rates? *Sci. Adv.* 2 (11), e1601542.
- Lavé, J., Burbank, D., 2004. Denudation processes and rates in the Transverse Ranges, southern California: erosional response of a transitional landscape to external and anthropogenic forcing. *Journal of Geophysical Research: Earth Surface* 109 (F1).
- Lee, S., Choi, J., 2004. Landslide susceptibility mapping using GIS and the weight-of-evidence model. *Int. J. Geogr. Inf. Sci.* 18 (8), 789–814.
- Lee, S., Choi, J., Min, K., 2002. Landslide susceptibility analysis and verification using the Bayesian probability model. *Environ. Geol.* 43 (1–2), 120–131.
- Marcher, M.V., 1969. Reconnaissance of the water resources of the Fort Smith Quadrangle, East-Central Oklahoma: Oklahoma Geological Survey Hydrologic Atlas, 1(4).
- Mathew, J., Jha, V., Rawat, G., 2007. Weights of evidence modelling for landslide hazard zonation mapping in part of Bhagirathi valley, Uttarakhand. *Current Science* 628–638.
- McGuire, L.A., Pelletier, J.D., Roering, J.J., 2014. Development of topographic asymmetry: insights from dated cinder cones in the western United States. *J. Geophys. Res.-Earth* 119 (8), 1725–1750.
- McKean, J., Roering, J., 2004. Objective landslide detection and surface morphology mapping using high-resolution airborne laser altimetry. *Geomorphology* 57 (3–4), 331–351.
- Meier, M., Post, A., Krimmel, R., Driedger, C., 1984. The 1983 recession of Columbia Glacier. US Geological Survey Open-File Report 84–59.
- Montgomery, D.R., Dietrich, W.E., 1988. Where do channels begin. *Nature* 336 (6196), 232–234.
- Oakes, M.C., 1952. Landslides in Le Flore County. Oklahoma Geological Survey Publication 12, 7–8.
- Ohlmacher, G.C., Davis, J.C., 2003. Using multiple logistic regression and GIS technology to predict landslide hazard in northeast Kansas, USA. *Eng. Geol.* 69 (3–4), 331–343.
- Oklahoma Climatological Survey, 2018. Climate of Oklahoma. https://climate.ok.gov/index.php/site/page/climate_of_oklahoma.
- Palumbo, L., Hetzel, R., Tao, M., Li, X., 2011. Catchment-wide denudation rates at the margin of NE Tibet from in situ-produced cosmogenic ¹⁰Be. *Terra Nova* 23 (1), 42–48.
- Pelletier, J.D., Barron-Gafford, G.A., Breshears, D.D., Brooks, P.D., Chorover, J., Durcik, M., Harman, C.J., Huxman, T.E., Lohse, K.A., Lybrand, R., Meixner, T., McIntosh, J.C., Papuga, S.A., Rasmussen, C., Schaap, M., Swetnam, T.L., Troch, P.A., 2013. Coevolution of nonlinear trends in vegetation, soils, and topography with elevation and slope aspect: a case study in the sky islands of southern Arizona. *J. Geophys. Res.-Earth* 118 (2), 741–758.
- Peng, Z., Vidale, J.E., Wech, A.G., Nadeau, R.M., Creager, K.C., 2009. Remote triggering of tremor along the San Andreas Fault in central California. *Journal of Geophysical Research: Solid Earth* (B7), 114.
- Peng, Z., Walter, J.I., Aster, R.C., Nyblade, A., Wiens, D.A., Anandkrishnan, S., 2014. Antarctic earthquakes triggered by the 2010 Maule earthquake in Chile. *Nat. Geosci.* 7 (9), 677.
- Poulos, M.J., Pierce, J.L., Flores, A.N., Benner, S.G., 2012. Hillslope asymmetry maps reveal widespread, multi-scale organization. *Geophys. Res. Lett.* 39.
- Regmi, N., Giardino, J., Vitek, J., 2013. Characteristics of landslides in western Colorado, USA. *Landslides* 1–15.
- Regmi, N.R., 2010. Hillslope Dynamics in the Paonia-McClure Pass Area, Colorado. USAPhD. Texas A&M University, College Station, TX.
- Regmi, N.R., Rasmussen, C., 2018. Predictive mapping of soil-landscape relationships in the arid Southwest United States. *Catena* 165, 473–486.
- Regmi, N.R., Giardino, J.R., Vitek, J.D., 2010a. Modeling susceptibility to landslides using the weight of evidence approach: Western Colorado, USA. *Geomorphology* 115 (1–2), 172–187.
- Regmi, N.R., Giardino, J.R., Vitek, J.D., Dangol, V., 2010b. Mapping landslide hazards in western Nepal: comparing qualitative and quantitative approaches. *Environmental & Engineering Geoscience* 16 (2), 127–142.
- Regmi, N.R., Giardino, J.R., Vitek, J.D., 2014a. Characteristics of landslides in western Colorado, USA. *Landslides* 11 (4), 589–603.
- Regmi, N.R., McDonald, E.V., Bacon, S.N., 2014b. Mapping Quaternary alluvial fans in the southwestern United States based on multiparameter surface roughness of lidar topographic data. *Journal of Geophysical Research: Earth Surface* 119 (1), 12–27 2012JF002711.
- Rodriguez, C., Bommer, J., Chandler, R., 1999. Earthquake-induced landslides: 1980–1997. *Soil Dyn. Earthq. Eng.* 18 (5), 325–346.
- Roering, J.J., Kirchner, J.W., Dietrich, W.E., 1999. Evidence for nonlinear, diffusive sediment transport on hillslopes and implications for landscape morphology. *Water Resour. Res.* 35 (3), 853–870.
- Roering, J.J., Perron, J.T., Kirchner, J.W., 2007. Functional relationships between denudation and hillslope form and relief. *Earth Planet. Sci. Lett.* 264 (1–2), 245–258.
- Seed, H.B., Chan, C.K., 1966. Clay strength under earthquake loading conditions. *Journal of Soil Mechanics & Foundations Div* 92 (2), 53–78 92(ASCE# 4723 Proceeding).
- Tucker, G.E., Hancock, G.R., 2010. Modelling landscape evolution. *Earth Surf. Process. Landf.* 35 (1), 28–50.
- Van Der Elst, N.J., Brodsky, E.E., 2010. Connecting near-field and far-field earthquake triggering to dynamic strain. *Journal of Geophysical Research: Solid Earth* 115 (B7).
- Van Westen, C., Rengers, N., Soeters, R., 2003. Use of geomorphological information in indirect landslide susceptibility assessment. *Nat. Hazards* 30 (3), 399–419.
- Varnes, D.J., 1978. *Soil Movement Types and Processes*. Special report. 176 pp. 11–33.
- Walsh, F.R., Zoback, M.D., 2015. Oklahoma's recent earthquakes and saltwater disposal. *Sci. Adv.* 1 (5), e1500195.
- Walter, J.I., Chang, J.C., Dotray, P.J., 2017. Foreshock seismicity suggests gradual differential stress increase in the months prior to the 3 September 2016 M_w 5.8 Pawnee earthquake. *Seismol. Res. Lett.* 88 (4), 1032–1039.
- Webb, P.K., 1960. Geology of the Cavanal Syncline, Le Flore County, Oklahoma Oklahoma.
- Yeck, W., Hayes, G., McNamara, D.E., Rubinstein, J.L., Barnhart, W., Earle, P., Benz, H.M., 2017. Oklahoma experiences largest earthquake during ongoing regional wastewater injection hazard mitigation efforts. *Geophys. Res. Lett.* 44 (2), 711–717.